

Advanced Functional Materials

Advanced lithium-sulfur batteries enabled by a bio-inspired polysulfide adsorptive brush

--Manuscript Draft--

| | |
|---|--|
| Manuscript Number: | adfm.201604069R1 |
| Full Title: | Advanced lithium-sulfur batteries enabled by a bio-inspired polysulfide adsorptive brush |
| Article Type: | Full Paper |
| Section/Category: | |
| Keywords: | lithium-sulfur batteries; brush-like interlayer; zinc oxide nanowires; conductive frameworks; polysulfides |
| Corresponding Author: | Vasant Kumar University of Cambridge UNITED KINGDOM |
| Additional Information: | |
| Question | Response |
| Please submit a plain text version of your cover letter here. If you are submitting a revision of your manuscript, please do not overwrite your original cover letter. There is an opportunity for you to provide your responses to the reviewers later; please do not add them here. | Dear Dr. Yuan, Thank you for forwarding the reviewers comments on our manuscript (IDadfm.201604069) entitled Advanced lithium-sulfur batteries enabled by a bio-inspired polysulfide adsorptive brush. We have considered all reviewers valuable comments and heuristic suggestions carefully and made revisions to the manuscript accordingly. If you have any further questions concerning the revised manuscript, please contact me without hesitation. Attached is our detailed reply to the comments of each of the reviewer. The replies appear in the order of the comments. Best regards, R. Vasant Kumar |
| Corresponding Author Secondary Information: | |
| Corresponding Author's Institution: | University of Cambridge |
| Corresponding Author's Secondary Institution: | |
| First Author: | Teng Zhao |
| First Author Secondary Information: | |
| Order of Authors: | Teng Zhao |
| | Yusheng Ye |
| | Xiaoyu Peng |
| | Giorgio Divitini |
| | Hyun-Kyung Kim |
| | Cheng-Yen Lao |
| | Paul R Coxon |
| | Kai Xi |
| | Yingjun Liu |
| | |

| | |
|--|---|
| | Caterina Ducati |
| | Renjie Chen |
| | Vasant Kumar |
| Order of Authors Secondary Information: | |
| Abstract: | <p>Issues with the dissolution and diffusion of polysulfides in liquid organic electrolytes hinder the advance of lithium-sulfur batteries for next-generation energy storage. To trap and reutilize the polysulfides without hampering lithium-ion conductivity, a bio-inspired brush-like interlayer consisting of zinc oxide (ZnO) nanowires and interconnected conductive frameworks is proposed. The chemical effect of ZnO on capturing polysulfides has been conceptually confirmed, initially by using a commercially-available macroporous nickel foam as a conductive backbone, which was then further replaced by a free-standing ultra-light micro/mesoporous carbon nanofiber mat for practical application. Having a high S loading of 3 mg cm⁻², the S/MWCNT composite cathode with a ZnO/C interlayer exhibited a reversible capacity of 776 mAh g⁻¹ after 200 cycles at 1C with only a 0.05 % average capacity loss per cycle. A good cycle performance at a high rate can be mainly attributed to the strong chemical bonding between ZnO and polysulfides, fast electron transfer and an optimized ion diffusion path arising from a well-organized nano-architecture. These results herald a new approach to advanced lithium-sulfur batteries using brush-like chemi-functional interlayers.</p> |

DOI: 10.1002/ ((please add manuscript number))

Article type: Full paper

Advanced lithium-sulfur batteries enabled by a bio-inspired polysulfide adsorptive brush

Teng Zhao[‡], Yusheng Ye[‡], Xiaoyu Peng[‡], Giorgio Divitini, Hyun-Kyung Kim, Cheng-Yen Lao, Paul R Coxon, Kai Xi, Yingjun Liu, Caterina Ducati, Renjie Chen, R. Vasant Kumar**

T. Zhao, Dr. X. Peng, Dr. G. Divitini, Dr. H. K. Kim, C. Lao, Dr. P. R Coxon, Dr. K. Xi, Dr. Y. Liu, Dr. C. Ducati, Dr. R. V. Kumar

Department of Materials Science and Metallurgy

University of Cambridge,

Cambridge, CB3 0FS, United Kingdom

E-mail: rvk10@cam.ac.uk.

Y. Ye, Prof. R. Chen

School of Materials Science and Engineering

Beijing Institute of Technology,

Beijing, 100081, China

E-mail: chenrj@bit.edu.cn.

Keywords: lithium-sulfur batteries, brush-like interlayer, zinc oxide nanowires, conductive frameworks, polysulfides

Abstract

1
2
3 Issues with the dissolution and diffusion of polysulfides in liquid organic electrolytes hinder
4
5 the advance of lithium-sulfur batteries for next-generation energy storage. To trap and re-
6
7 utilize the polysulfides without hampering lithium-ion conductivity, a bio-inspired brush-like
8
9 interlayer consisting of zinc oxide (ZnO) nanowires and inter-connected conductive
10
11 frameworks is proposed. The chemical effect of ZnO on capturing polysulfides has been
12
13 conceptually confirmed, initially by using a commercially-available macroporous nickel foam
14
15 as a conductive backbone, which was then further replaced by a free-standing ultra-light
16
17 micro/mesoporous carbon nanofiber mat for practical application. Having a high S loading of
18
19 3 mg cm⁻², the S/MWCNT composite cathode with a ZnO/C interlayer exhibited a reversible
20
21 capacity of 776 mAh g⁻¹ after 200 cycles at 1C with only a 0.05 % average capacity loss per
22
23 cycle. A good cycle performance at a high rate can be mainly attributed to the strong chemical
24
25 bonding between ZnO and polysulfides, fast electron transfer and an optimized ion diffusion
26
27 path arising from a well-organized nano-architecture. These results herald a new approach to
28
29 advanced lithium-sulfur batteries using brush-like chemi-functional interlayers.
30
31
32
33
34
35
36
37
38
39
40
41
42
43
44
45
46
47
48
49
50
51
52
53
54
55
56
57
58
59
60
61
62
63
64
65

1. Introduction

1 Sulfur (S) is an attractive cathode material for the next-generation high-energy rechargeable
2 lithium (Li) batteries.^[1-4] Owing to its low atomic number and two-electron transfer capability
3
4 with Li, S offers a theoretical specific capacity of 1672 mAh g⁻¹. With an operational voltage
5
6 of 2.1 V, the overall available energy density of Li-S batteries is five times that of state-of-
7
8 the-art LIBs. In addition, the non-toxic nature and abundance of S are also attractive in terms
9
10 of large-scale production and, more importantly, sustainable development which is a crucial
11
12 factor in mass deployment of electrical vehicles.
13
14
15
16

17
18 Despite their obvious advantages, the reality of producing practical Li-S batteries is dogged
19
20 by challenges. Three critical problems arise from sulfur's inherent chemistry. First,
21
22 orthorhombic S₈, the most stable form of elemental S in nature, has poor electrochemical
23
24 accessibility with a low conductivity of 5×10⁻²⁸ S m⁻¹ at room temperature, which results in
25
26 low active material utilization. Second, several kinds of intermediate polysulfides with
27
28 various molecular lengths are produced by the multi-step electrochemical reactions involved
29
30 in the normal operation of a battery.^[5-7] Among them, long-chain polysulfides (Li₂S_x, 4≤x<8)
31
32 easily dissolve in organic solvents and diffuse to the anode, where they react with Li to form
33
34 short-chain polysulfides (Li₂S_x, 1<x<4). Some of these, such as Li₂S₂, precipitate and then
35
36 deposit on the surface of the lithium anode, causing irreversible loss of active materials;
37
38 others diffuse back and are re-oxidized at the cathode, leading to the notorious “redox shuttle”
39
40 and hinder Coulombic efficiency.^[8] Last but not least, the volume change of the S cathode
41
42 during cycling, caused by the density difference between S and the final discharge product
43
44 Li₂S, is also of concern, since it causes serious pulverization of the cathode and leads to
45
46 capacity degradation.^[9-11]
47
48
49
50
51
52

53 Approaches for addressing these performance-related problems have been developed over
54
55 decades, including the design of conductive S hosts,^[4, 12-17] functional electrolyte additives,^{[18-}
56
57
58
59
60
61
62
63
64
65
20] anode protection^[21-23] and new cell configurations.^[24-28] Recently, considerable effort has

1
2
3
4
5
6
7
8
9
10
11
12
13
14
15
16
17
18
19
20
21
22
23
24
25
26
27
28
29
30
31
32
33
34
35
36
37
38
39
40
41
42
43
44
45
46
47
48
49
50
51
52
53
54
55
56
57
58
59
60
61
62
63
64
65

been made to find a chemical route to effectively trap migrating polysulfides and ensure good cycle life.^[29] One possible way is to encapsulate S in a modified carbon matrix, such as graphene oxide,^[30] N-doped porous carbon,^[31-33] B-doped/ S, N dual doped graphene,^[34-36] whose asymmetry surface charge can enhance the chemical binding with polar polysulfides. However, it is challenging to get a strong chemical interaction without sacrificing the conductivity of carbon backbone by introducing functional groups or heteroatoms doping. Another promising approach is to use nano-structured metal oxides as polysulfides adsorbents. Initially, porous nano-structured metal oxides, such as Al₂O₃,^[37] SiO₂,^[38] were directly used as an additive in cathode, offering on-site adsorption of polysulfides, but these scattered absorption sites cannot ensure high active utilization due to the semi-conductive nature of metal oxides. Very recently, it has been found that metal oxides with suitable redox potential have strong chemical interaction with polysulfides through their polar surface/surface redox reaction.^[39, 40] For example, MnO₂ nano sheet has been used as a coating layer to structurally and chemically encapsulate polysulfides.^[41, 42] Based on the analysis on previous researches, we propose that building a well-organized metal oxide nano-architecture on an interconnected conductive network could further optimize the chemical effect of metal oxides on confining polysulfides.

Inspired by the brush-like membrane of cells for nutrient adsorption, a similar structure of interlayer consisting of zinc oxide nanowires and conductive frameworks has been designed for chemical adsorption of polysulfides in organic electrolytes. A proof of concept for polysulfides adsorptive brush has been initially demonstrated by sandwiching a sulfur/carbon nanotube cathode with a zinc oxide nanowires/nickel foam interlayer, as this configuration is readily achieved with the appropriate pore morphology, adsorption ability and structure stability. The chemical role of zinc oxide nanowires in anchoring polysulfides has been revealed by the analysis of the morphology and composition of cycled interlayer as well as the theoretical DFT calculation of binding energy of ZnO and five relevant S-based species.

1 Based upon the successful demonstration, a functional and much lighter and thinner interlayer
2 has been made by integrating ZnO nanowires with a carbon nanofiber mat for practical
3 application of Li-S batteries. The porous carbon nanofiber backbone with large specific
4 surface area serves as a sponge to draw polysulfides into the chemical channels between ZnO
5 nanowires. And its interconnected conductive network and thin thickness ensure fast electron
6 transfer and ion diffusion. With the incorporation of this brush-like ZnO/C interlayer, a
7 S/MWCNT cathode exhibited a stable cycle performance with only 0.05% average capacity
8 loss per cycle after 200 cycles at a relatively high current rate of 1C ($1C=1672\text{mAh g}^{-1}$). The
9 design of chemi-functional interlayers with brush-like nano-architecture opens a new
10 direction for trapping and re-utilizing polysulfide without hampering ion conductivity.

24 2. Results and Discussion

25 To give a proof of concept for polysulfides adsorptive brush, zinc oxide nanowires were
26 initially grown on a commercially-available nickel foam and this combination was
27 sandwiched with a S/MWCNT composite cathode. Considering its limited physical adsorption
28 properties and robustness for postmortem analysis after cycling, Ni foam is an ideal substrate
29 to investigate the chemical effect of ZnO on soluble polysulfides. **Figure 1a** shows the
30 schematic configuration of the Li-S cell with the prototypical ZnO nanowires/Ni foam
31 interlayer. A S/MWCNT composite was prepared according to the previously reported
32 thermal infusion method.^[12] S was uniformly coated on the surface of CNTs to form a core-
33 shell structure. (**Figure S1**). The characteristic peaks of orthorhombic S₈ in the X-ray
34 diffraction (XRD) spectrum of the S/MWCNT composite confirms the crystalline nature of S
35 deposited on the MWCNT host (**Figure S2**). Raman measurements shown in **Figure S3** also
36 indicate that there was no chemical bonding between S and MWCNT, proving that S was
37 physically attached to the MWCNT. For practical applications, the content of S in the
38 composite was tailored to be 70% wt (**Figure S4**), while the area density was about 3 mg cm^{-2} .

39 In addition, the thickness of the S/MWCNT composite cathode was about $100\mu\text{m}$ (**Figure S5**).

1 The ZnO nanowires/Ni foam interlayer was sandwiched with the S/MWCNT composite
2 cathode and placed in front facing the separator. The growth of ZnO nanowires on the Ni
3
4 foam was achieved through chemical bath deposition.^[43] XRD was undertaken to investigate
5
6 the crystal phase of the hybrid ZnO nanowires/Ni foam interlayer. As shown in **Figure S6**,
7
8 except for the distinct peaks assigned to Ni, the residual peaks were unambiguously indexed
9
10 as the hexagonal wurtzite phase of ZnO. **Figure 1b-c** show the top-view and cross-section
11
12 scanning electron microscopy (SEM) images of the ZnO nanowires/Ni foam interlayer. The
13
14 3D macroporous structure of Ni foam, with a thickness of 500 μm , can be clearly seen from
15
16 low magnification images. Closer SEM observations at much higher magnification reveal the
17
18 1D nano architecture of ZnO, covering each strip of Ni foam with features having a diameter
19
20 of 150 nm and a length of 2.5 μm (**Figure 1d-f**). Electron energy dispersive spectroscopy
21
22 (EDS) (**Figure 1g**) further confirms the uniform distribution of ZnO nanowires on the 3D
23
24 macroporous structure of the Ni foam. **Based on the analysis of mass change of interlayer**
25
26 **before and after ZnO growth, the areal loading of ZnO on the Ni foam was determined to be**
27
28 **about 6 mg cm⁻².** Thus, a unique structure is created by combining locally high surface area
29
30 1D ZnO nanowire arrays grown and anchored in a brush-like morphology on a large pore
31
32 volume 3D Ni foam for optimizing chemical interaction with the soluble polysulfides from
33
34 the electrolyte-solvent.
35

36
37 To directly demonstrate the polysulfides capture capability of ZnO nanowires, the hybrid
38
39 interlayer was recovered from the fully charged coin cell after 500 deep cycles at 2C and its
40
41 morphology was characterized by TEM after repeated washing with 1,2-dimethoxyethane
42
43 (DME). **Figure 2a** shows the ultra-long cycle performance of S/MWCNT cathodes with ZnO
44
45 nanowires/Ni foam interlayer at 2C. A reversible capacity of 577.1 mAh g⁻¹ with a capacity
46
47 retention of 81% was achieved after 500 cycles, although a small capacity degradation and
48
49 low Coulombic efficiency were observed in the initial 10 cycles at high rates, which could be
50
51 due to the sluggish conversion from inactive solid Li₂S to S. **Figure 2b-c** shows the TEM
52
53
54
55
56
57
58
59
60
61
62
63
64
65

1 images of ZnO nanowires detached from the cycled hybrid interlayer by ultra-sonication. It
2 can be seen that a new fairly rough layer was coated on each nanowire to form a core-shell
3 structure and the average thickness of the coating shell was approximately 30 nm; EDS
4 mapping further confirms this shell as S-containing species anchored on the surface of ZnO
5 nanowires, which provides direct evidence for the role of ZnO in trapping polysulfides.
6

7
8
9
10
11 The chemical composition of S species was investigated by X-ray photoelectron spectroscopy
12 (XPS). **Figure 2d** compares the XPS survey spectra of the ZnO nanowires/Ni foam interlayer
13 before and after cycling. The intensity of Zn signals from ZnO was markedly reduced with the
14 appearance of S signal in the spectrum after cycling, which agrees well with the coating of S
15 species on the ZnO surface. No other signals such as F, N, were detected in the surveyed
16 spectrum of the cycled hybrid interlayer, which indicates that electrolyte salt was completely
17 removed from the robust structure of the cycled ZnO nanowires/Ni foam interlayer after an
18 intense and a thorough wash and the observed S signals mainly arise from the migrated active
19 materials. **Figure 2e** show the S 2p XPS spectra of the cycled hybrid interlayer. It can be seen
20 that four S-containing species were identified, including Li_2S_2 (162.6 eV, 162.1 eV), S_8 (164.1
21 eV, 163.2 eV), thiosulfate (167.2 eV) and polythionate complex (169.7 eV, 168.7 eV). The
22 deposition of discharge product Li_2S_2 cannot be avoided due to its insulating nature and poor
23 electrochemical reversibility. Because of the lower redox potential of ZnO than that of
24 polysulfides,^[39, 44] the generated thiosulfate/polythionate complex could mainly come from
25 the oxidation of polysulfides by LiNO_3 , which is a common additive in the electrolyte to
26 mitigate the polysulfides shuttle effect.^[45] **Except S_8 , other S-containing species can not be
27 electrochemically reutilized, but thiosulfate and polythionate can act as a polysulfide mediator
28 to chemically curtail active loss during charge and discharge process.**^[40] **Figure 2f** compares
29 the Zn 2p_{3/2} XPS spectra of ZnO/C interlayer before and after cycle. It can be seen that a slight
30 binding energy shift of Zn 2p_{3/2} from 1021 eV to 1020.5 eV after cycling was observed,
31 reflecting the chemical interaction between ZnO and S species.
32
33
34
35
36
37
38
39
40
41
42
43
44
45
46
47
48
49
50
51
52
53
54
55
56
57
58
59
60
61
62
63
64
65

To give further insight into the chemical confining effect of ZnO on polysulfides, the binding energy (E_b) of five most relevant S species (Li_2S_n) on the polar O-terminated surface of ZnO was calculated using density functional theory (DFT) because the strong binding of metal oxide and lithium polysulfides mainly originates from Li-O interaction according to the previous reports^[41, 46]. The E_b is defined as $E(\text{ZnO})+E(\text{Li}_2\text{S}_n)-E(\text{ZnO}/\text{Li}_2\text{S}_n)$, where $E(\text{ZnO})$, $E(\text{Li}_2\text{S}_n)$ and $E(\text{ZnO}/\text{Li}_2\text{S}_n)$ are total energy of isolated ZnO, Li_2S_n , and ZnO bound to a Li_2S_n , respectively. As shown in **Figure 2g**, the E_b value for Li_2S_8 remarkably reaches 3.98 eV, which is one the highest reported for similar systems.^[47] With a decrease in molecular length of polysulfides, the corresponding E_b reduces to a lowest value of 1.26 eV for Li_2S_4 due to the limited interaction area. After that, E_b gradually increases to 2.70 eV for Li_2S , which could be explained by the enhanced interaction between the O-terminated surface and short-chain polysulfides due to similar polarity.

Once the concept of polysulfide adsorptive brush is proven, the next task is to replace the high density Ni foam with a light, porous material, fabricated such that it has a suitable microstructure to maximize the area of “brush border”. Considering their tightly interwoven architecture and tunable thickness, free-standing carbon nanofiber mats have been chosen as a desirable substrates for ZnO growth (**Figure 3a**). PAN nanofiber precursor was first prepared by electrospinning, followed by stabilizing in air and carbonizing and activating in low oxygen-containing N_2 . Thereafter, zinc oxide nanowires were grown on the as-prepared carbon nanofiber using the chemical bath method described earlier. **Figure 3b and 3c** show the cross-section SEM images of carbon nanofiber mats. A layered structure with a thickness of approximately 50 μm is observed and the space between these loosely stacked layers is favorable for the infiltration of ZnO growth solution. From the SEM images shown in **Figure 3d-3e**, it can be seen that the black carbon mat has a fish-net micro-structure formed by the interconnection of individual carbon nanofiber with an average diameter of 200 nm. After the uniform growth of ZnO nanowires on each carbon nanofiber, a fluffy and brush like

1
2
3
4
5
6
7
8
9
10
11
12
13
14
15
16
17
18
19
20
21
22
23
24
25
26
27
28
29
30
31
32
33
34
35
36
37
38
39
40
41
42
43
44
45
46
47
48
49
50
51
52
53
54
55
56
57
58
59
60
61
62
63
64
65

architecture was achieved (**Figure 3f**), which caused a decrease in the BET specific area from $600 \text{ m}^2 \text{ g}^{-1}$ to $192 \text{ m}^2 \text{ g}^{-1}$ (**Figure S7**). From a closer observation, the decorated ZnO nanowire has a diameter of $\sim 50 \text{ nm}$ and a length of $\sim 500 \text{ nm}$ (**Figure 3g**). In addition, its wurtzite crystal structure was evidenced by XRD (**Figure S8**) and the content of ZnO in the hybrid interlayer was 55% wt based on the results of TGA, corresponding to an areal loading of 0.7 mg cm^{-2} (**Figure S9**).

The effects of the hybrid ZnO/C interlayer on the electrochemical performance of Li-S cell were investigated using S/MWCNT composite as cathode and Li as anode. To ensure the same sulfur content considering the combined mass of cathode and interlayer, a S/MWCNT composite cathode with a $\sim 110 \text{ }\mu\text{m}$ -thick carbon nanofiber interlayer was tested for reference. Initially, electrochemical impedance was measured at open circuit potential (OCP) of cells to characterize the internal resistance. The Nyquist plots of S/WMCNT composite cathode with different interlayers were displayed in **Figure S10**. Interestingly, it was found that both samples had a similar charge transfer resistance (R_{ct}) of approximately 45Ω , which could be attributed to the equivalent effect of introduction of semi-conductor ZnO and increase in the thickness on the conductivity of carbon nanofiber interlayer. **Figure 4a** compares the cycle performance of S/MWCNT composite cathode with two different interlayers at a current rate of 0.2C. For S/MWCNT cathode with a ZnO/C interlayer, it reached an initial discharge capacity of $1084.7 \text{ mAh g}^{-1}$, corresponding to a S utilization of 64.8%. After 50 cycles, a reversible capacity remained high at $1030.7 \text{ mAh g}^{-1}$ with a capacity retention of 95%. In controlled experiment, S/MWCNT cathode with carbon nanofiber interlayer exhibited a slightly lower S utilization (58.8%) for the first cycle, but its capacity retention after 50 cycles was only 68.8%. Thus, the hybrid ZnO/C interlayer led to better cycle performance. **Figure 4b and 4c** shows the discharge-charge profiles of S/MWCNT cathode with different interlayers in the 1st, 5th and 50th cycle, respectively. The distinct two-plateau discharge behavior was observed in all profiles, which is the typical electrochemical features of S. At

1 high and steep plateau around potential of 2.3V, cyclo-S₈ is converted to long-chain
2 polysulfides Li₂S_n (4<n<8). As discharge proceeds onward, short-chain polysulfides Li₂S_n
3 (2<n<4) and even solid Li₂S₂/Li₂S are formed at long and planar plateau around potential of
4 2.1V. Notably, S/MWCNT cathode with ZnO/C interlayer exhibited less potential hysteresis
5 with cycling compared with the control sample. In addition, the position and intensity of redox
6 peaks in the cyclic voltammetry (CV) curves of S/MWCNT cathode with ZnO/C interlayer
7 also showed minimal changes during the first three cycles, suggesting that ZnO enhanced the
8 reversibility of S redox reaction (**Figure S11**).

9
10
11
12
13
14
15
16
17
18
19 The long cycle performance of S/MWCNT cathodes with two different interlayers at a high
20 current rate of 1C is plotted in **Figure 4d**. Compared with the performance at 0.2C, reduced S
21 utilization and capacity stability were observed for both samples during the initial 50 cycles at
22 1C. **Generally, the utilization of sulfur mainly depends on two factors: (1) intimate contact**
23 **with conductive framework; (2) effective confinement of soluble intermediate polysulfide.**
24 **When it comes to a high current rate, kinetics of S redox and ion diffusion are also of great**
25 **concern.** S/MWCNT cathode with ZnO/C interlayer delivered an initial capacity of 867.6
26 mAh g⁻¹, which gradually reduced to 787.6 mAh g⁻¹ after 50 cycles with a capacity retention
27 of 90.7%. After 200 cycles, a reversible capacity of 776 mAh g⁻¹ was achieved, corresponding
28 to only 0.05% average capacity loss per cycle. In contrast, the initial capacity of S/MWCNT
29 cathode with C interlayer at 1C was much lower (512.7mAh g⁻¹), about 60% of that of
30 S/MWCNT cathode with ZnO/C interlayer, followed by a rapid decay to 287.5 mAh g⁻¹ at 50
31 cycles. The corresponding capacity retention was 56%. With the slow infiltration of
32 electrolyte in the thick C interlayer, the capacity gradually increased after 50 cycles and
33 maintained at 333.5 mAh g⁻¹ after 200 cycles with 0.17% average capacity loss per cycle.
34
35
36
37
38
39
40
41
42
43
44
45
46
47
48
49
50
51
52
53
54
55
56 **Figure 4e and 4f** display the discharge-charge profiles of the S/MWCNT cathode with
57 different interlayers in the 1st, 5th and 200th cycle, respectively. It can be seen that the system
58 with the incorporation of ZnO/C interlayer exhibited much better rate stability, with negligible
59
60
61
62
63
64
65

1 change in plateau potential with cycling. To our best knowledge, this is the first report using a
2 brush-like interlayer to achieve a high S utilization and excellent capacity retention at both
3
4 low and high current rates for a cathode with a S loading of 3 mg cm^{-2} (**Table S1**). In addition,
5
6 a good capacity and cycle stability were observed when the S loading was further increased to
7
8
9 5.2 mg cm^{-2} (**Figure S12**).

10
11 The unique brush-like structure of ZnO/C interlayer mainly contributed to the superior
12
13 electrochemical performance. As shown in **Figure 5a**, the self-organized zinc oxide
14
15 nanowires forms a “brush border” on carbon nanofiber, which increases the contact area for
16
17 electrolytes. And individual zinc oxide nanowire acts as “microvilli” to chemically adsorb the
18
19 dissolved polysulfides in electrolytes. The whole capture process of migrating polysulfides
20
21 mimics the adsorption of nutrients in intestinal cells. Meanwhile, the carbon nanofiber mat
22
23 provides interconnected conductive network for reutilizing polysulfides and its thin thickness
24
25 ensures trapping polysulfides without hampering lithium ion conductivity. To better
26
27 understand the function of this brush-like ZnO/C interlayer, elemental distribution mapping
28
29 on both sides of cycled ZnO/C interlayer after 200 cycles at 1C was conducted using EDS. As
30
31 shown in **Figure 5b and 5c**, it can be seen that intense S signal were detected on the side
32
33 facing cathode, directly evidencing that ZnO/C interlayer had the capability of anchoring and
34
35 reutilizing migrating polysulfides. On the other hand, the S signal was weak on the side facing
36
37 the separator. **The semi-quantitative calculation of the amount of S anchored on the different**
38
39 **sides of brush-like interlayer was carried out based on the corresponding EDS spectra shown**
40
41 **in Figure S13. It was found the atomic ratio of S to Zn on the cathode side was about 5 times**
42
43 **higher than that on the anode side, implying that most dissolved polysulfides were adsorbed by**
44
45 **this thin interlayer.**

56 3. Conclusions

57
58 In conclusion, we have demonstrated a good cycle and rate performance of Li-S batteries
59
60 using a zinc oxide nanowire based brush-like interlayer. ZnO nanowires play the key role in
61

1 adsorbing migrating polysulfides due to a strong chemical bonding and their well-organized
2 brush-like nano-architecture built on thin and interconnected conductive framework, which
3
4 mimics the microstructure of intestinal cells, further enhances the effectiveness of
5 polysulfides adsorption and reutilization process by affording fast electron and ion motion.
6
7 Thanks to the bio-inspired ZnO/C interlayer, the S/MWCNT composite cathode with a high S
8
9 loading of 3 mg cm^{-2} maintained a reversible capacity of 776 mAh g^{-1} after 200 cycles at 1C,
10
11 corresponding a 0.05 % average capacity loss per cycle. Building chemi-functional interlayers
12
13 with brush-like nano-architecture will leads to a new approach for advancing high-
14
15 performance Li-S batteries in the near future. And the integration of nanostructured metal
16
17 oxides with conductive frameworks is also a versatile strategy to fabricate hierarchically
18
19 multi-functional materials for a wide range of applications.
20
21
22
23
24
25

26 **4. Experimental section**

27
28
29 *Chemical bath deposition of ZnO nanowire arrays on nickel foam:* Commercially-purchased
30
31 nickel foams were pressed and cut into circular disks with an average diameter of 11 mm and
32
33 thickness of 0.5 mm, followed by rinsing with deionized water and ethanol. Prior to the
34
35 growth of nanowire arrays, a piece of treated Ni foam was initially wet with several droplets
36
37 of 0.005M zinc acetate dehydrate ($\text{Zn}(\text{CH}_3\text{COO})_2 \cdot 2\text{H}_2\text{O}$) in ethanol and then annealed at 300
38
39 °C to form a seeding layer of ZnO nano crystals. This seeding treatment was repeated three
40
41 times. The ZnO-seeded Ni foam was then put in a 20 ml aqueous solution of 0.05 M zinc
42
43 nitrate ($\text{Zn}(\text{NO}_3)_2 \cdot 6\text{H}_2\text{O}$), 0.025 M, hexamethylenetetramine (HMTA), 0.45 M $\text{NH}_3 \cdot \text{H}_2\text{O}$ and
44
45 5mM polyethylenimine (PEI), followed by heating at 95 °C for 24h in an oven. Finally, the
46
47 sample was collected and rinsed repeatedly with deionized water. Calculated by the mass
48
49 change in the Ni foam before and after ZnO growth, the area density of ZnO nanowires was
50
51 approximately 6 mg cm^{-2} .
52
53
54
55
56
57

58 *Thermal infusion of S on the surface of MWCNT:* The core-shell structured S/MWCNT
59
60 composites were prepared using thermal infusion method. Briefly, 0.7g S was first mixed well
61
62
63
64
65

1 with 0.3g MWCNT (Specific surface area 160-200 m² g⁻¹, diameter 10-30 nm, length >2 μm,
2 purity>97%) and sealed in a polytetrafluoroethylene container under the protection of Ar gas,
3
4 which was then transferred to furnace and heated at 150 °C for 24h.
5
6

7 *Fabrication of electron-spun PAN derived carbon nanofiber:* 5g Polyacrylonitrile (PAN) with
8
9 an average molecular weight of Mw = 150,000 g/mol was dissolved in 9 ml N,N-
10 dimethylformamide (DMF) to form a 10 wt.% solution by constant stirring for 24h. Then, the
11 readily polymer solution was loaded into a syringe with a stainless nozzle (0.6 mm diameter)
12 for electrospinning process. The applied voltage was set at 20 kV, and the flow rate of
13 solution was 1 mL h⁻¹. The as-electrospun nanofibers with a thickness of ~50 μm were
14 collected with an aluminum foil (10 cm×10 cm) located 20 cm away from the tip of the
15 nozzle after 1h. The peeled PAN nanofiber was initially stabilized in air at 280 °C for 3h,
16 followed by carbonization and activation at 1000 °C under a low oxygen-containing nitrogen
17 atmosphere for 6 hours.
18
19
20
21
22
23
24
25
26
27
28
29
30

31 *Growth of ZnO nanowire on carbon nanofiber:* Zinc oxide nanowires were grown on the as-
32 prepared carbon nanofiber using the same chemical bath method, which were then cut into
33 circular disks with an average diameter of 11 mm and mass of ~1.3 mg cm⁻²
34
35
36
37
38

39 *Material Characterization:* Raman spectroscopy data was obtained on a Dilor XY-800
40 spectrometer using a 514 nm wavelength laser. X-ray diffraction analysis of samples was
41 carried out with a Bruker D8 advance powder X-ray diffractometer with a Cu Kα radiation
42 source; The morphology of samples was characterised by scanning electron microscopy (SEM,
43 FEI Nova NanoSEM, 5 kV) equipped with an energy dispersive X-ray spectrometer (EDS)
44 and transmission electron microscopy (FEI Tecnai Osiris and JEOL 2100F, 200 kV); XPS
45 measurements were performed at room temperature with a Kratos Analytical spectrometer
46 and monochromatic Al Kα (1486.6 eV) X-ray source. Thermal gravimetric analysis (TGA)
47 was conducted on a TA Instruments Q2000 thermal analyzer in air with a heating rate of
48 10 °C min⁻¹.
49
50
51
52
53
54
55
56
57
58
59
60
61
62
63
64
65

1
2
3
4
5
6
7
8
9
10
11
12
13
14
15
16
17
18
19
20
21
22
23
24
25
26
27
28
29
30
31
32
33
34
35
36
37
38
39
40
Electrochemical tests: The S cathode slurry was prepared by mixing the as-prepared S/MWCNT composite, carbon black and polyvinylidene fluoride (PVDF) binder at a ratio of 7:2:1 in N-methyl-2-pyrrolidinone (NMP), which was then spread on aluminum foil via doctor blade. The wet cathode was dried at 60 °C for 24hs to remove solvents and then cut into disc with a diameter of 11mm. Two-electrode coin cells (CR2025) were assembled in an argon-filled glove box for electrochemical measures using Li foil as the counter electrode and a microporous polyethylene separator. The ZnO/C interlayer was sandwiched with S/MWCNT composite cathode and placed in front facing the separator. The electrolyte used was 1.0 M bis-(trifluoromethane)sulfonimide lithium (LiTFSI) in a 1:1 v/v mixture of 1,2-dimethoxyethane (DME) and 1,3-dioxolane (DOL) with 0.2M lithium nitrate (LiNO₃). Galvanostatic charge/discharge tests were performed at different current densities between 1.8 V and 2.6 V vs Li/Li⁺ at room temperature by using a LAND-CT2001A (Wuhan, China). CV analysis was recorded on a CHI660c electrochemical workstation (Shanghai, Chenhua) between 1.8 V and 3.0 V to characterize the redox behavior and kinetic reversibility of the cells. Alternating-current (AC) impedance was measured for fresh cells at the OCP by using a CHI660C electrochemical workstation. The AC amplitude was ±5 mV, and the applied frequency range was from 100 kHz to 0.1 Hz.

41
42
43
44
45
46
47
48
49
50
51
52
53
54
55
56
57
58
59
60
61
62
63
64
65
Theoretical calculations: Theoretical calculations were performed using Materials Studio 5.5 (Accelrys). The atomic configurations and binding energies were calculated using DFT within the Perdew-Berke-Ernzerh functional of Generalized Gradient Approximation (GGA-PBE) basis set. A 7×7×2 supercell was employed to model ZnO and ZnO-Li₂S_n structures. Brillouin zone was sampled by a 2×1×1 k-point Monkhorst-Pack grid. An energy cutoff of 400.0 eV was used to describe the interactions. All atoms were fully relaxed when the following convergence tolerance was met: the residual forces on the constituent atoms became smaller than 0.03 eV/Å and the maximum atomic displacement was higher than 0.005 Å.

Supporting Information

Supporting Information is available from the Wiley Online Library or from the author.

Acknowledgements

T.Z. acknowledges the support of a Krishnan-Ang studentship from Trinity College, Cambridge. X.P., G.D. and C.D. acknowledge funding from ERC under grant number 259619 PHOTO EM. C.D. acknowledges financial support from the EU under grant number 312483 ESTEEM2. This work was also supported by the National Science Foundation of China (21373028), Major achievements Transformation Project for Central University in Beijing and Beijing Science and Technology Project (D151100003015001). T. Z., Y. Y. and X. P. contributed equally to this work.

Received: ((will be filled in by the editorial staff))

Revised: ((will be filled in by the editorial staff))

Published online: ((will be filled in by the editorial staff))

- [1] R. Chen, T. Zhao, F. Wu, *Chem. Commun.* **2015**, 51, 18.
- [2] S. Evers, L. F. Nazar, *Acc. Chem. Res.* **2013**, 46, 1135.
- [3] A. Manthiram, Y. Fu, S.-H. Chung, C. Zu, Y.-S. Su, *Chem. Rev.* **2014**, 114, 11751.
- [4] Y. Yang, G. Zheng, Y. Cui, *Chem. Soc. Rev.* **2013**, 42, 3018.
- [5] H. Yamin, A. Gorenshtein, J. Penciner, Y. Sternberg, E. Peled, *J. Electrochem. Soc.* **1988**, 135, 1045.
- [6] J. Xiao, J. Z. Hu, H. Chen, M. Vijayakumar, J. Zheng, H. Pan, E. D. Walter, M. Hu, X. Deng, J. Feng, B. Y. Liaw, M. Gu, Z. D. Deng, D. Lu, S. Xu, C. Wang, J. Liu, *Nano Lett.* **2015**, 15, 3309.
- [7] C. Barchasz, F. Molton, C. Duboc, J.-C. Leprêtre, S. Patoux, F. Alloin, *Anal. Chem.* **2012**, 84, 3973.
- [8] Y. V. Mikhaylik, J. R. Akridge, *J. Electrochem. Soc.* **2004**, 151, A1969.
- [9] R. Elazari, G. Salitra, Y. Talyosef, J. Grinblat, C. Scordilis-Kelley, A. Xiao, J. Affinito, D. Aurbach, *J. Electrochem. Soc.* **2010**, 157, A1131.
- [10] S.-E. Cheon, K.-S. Ko, J.-H. Cho, S.-W. Kim, E.-Y. Chin, H.-T. Kim, *J. Electrochem. Soc.* **2003**, 150, A796.
- [11] J. Nelson, S. Misra, Y. Yang, A. Jackson, Y. Liu, H. Wang, H. Dai, J. C. Andrews, Y. Cui, M. F. Toney, *J. Am. Chem. Soc.* **2012**, 134, 6337.
- [12] R. Chen, T. Zhao, J. Lu, F. Wu, L. Li, J. Chen, G. Tan, Y. Ye, K. Amine, *Nano Lett.* **2013**, 13, 4642.
- [13] X. Ji, K. T. Lee, L. F. Nazar, *Nat. Mater.* **2009**, 8, 500.
- [14] R. Chen, T. Zhao, T. Tian, S. Cao, P. R. Coxon, K. Xi, D. Fairen-Jimenez, R. Vasant Kumar, A. K. Cheetham, *APL Mater.* **2014**, 2, 124109.

- 1 [15] M. Zhao, Q. Zhang, J. Huang, G. Tian, J. Nie, H. Peng, F. Wei, *Nat. Commun.* **2014**, *5*, 3410.
2 [16] F. Wu, J. Chen, R. Chen, S. Wu, L. Li, S. Chen, T. Zhao, *J. Phys. Chem. C* **2011**, *115*, 6057.
3 [17] F. Wu, J. Chen, L. Li, T. Zhao, R. Chen, *J. Phys. Chem. C* **2011**, *115*, 24411.
4 [18] Z. Lin, Z. Liu, W. Fu, N. J. Dudney, C. Liang, *Adv. Funct. Mater.* **2012**, *23*, 1064.
5 [19] J.-S. Kim, T. H. Hwang, B. G. Kim, J. Min, J. W. Choi, *Adv. Funct. Mater.* **2014**, *24*, 5359.
6 [20] J. Kim, D. J. Lee, H. G. Jung, Y. K. Sun, J. Hassoun, B. Scrosati, *Adv. Funct. Mater.* **2013**, *23*,
7 1076.
8 [21] R. Cao, W. Xu, D. Lv, J. Xiao, J.-G. Zhang, *Adv. Energy Mater.* **2015**, *5*, 1402273.
9 [22] F. Wu, J. Qian, R. Chen, J. Lu, L. Li, H. Wu, J. Chen, T. Zhao, Y. Ye, K. Amine, *ACS Appl.*
10 *Mater. Interfaces* **2014**, *6*, 15542.
11 [23] A. C. Kozen, C.-F. Lin, A. J. Pearse, M. A. Schroeder, X. Han, L. Hu, S. B. Lee, G. W. Rubloff,
12 M. Noked, *ACS Nano* **2015**, *9*, 5884.
13 [24] Y.-S. Su, A. Manthiram, *Nat. Commun.* **2012**, *3*, 1166.
14 [25] H. Peng, D. Wang, J. Huang, X. Cheng, Z. Yuan, F. Wei, Q. Zhang, *Adv. Sci.* **2016**, *3*, 1500268
15 [26] S. Chung, A. Manthiram, *Adv. Funct. Mater.* **2014**, *24*, 5299.
16 [27] J. Balach, T. Jaumann, M. Klose, S. Oswald, J. Eckert, L. Giebeler, *Adv. Funct. Mater.* **2015**, *25*,
17 5285.
18 [28] J.-Y. Hwang, H. M. Kim, S.-K. Lee, J.-H. Lee, A. Abouimrane, M. A. Khaleel, I. Belharouak, A.
19 Manthiram, Y.-K. Sun, *Adv. Energy Mater.* **2015**, *6*, 1501480.
20 [29] M. Liu, F. Ye, W. Li, H. Li, Y. Zhang, *Nano Res.* **2016**, *9*, 94.
21 [30] L. Ji, M. Rao, H. Zheng, L. Zhang, Y. Li, W. Duan, J. Guo, E. J. Cairns, Y. Zhang, *J. Am. Chem.*
22 *Soc.* **2011**, *133*, 18522.
23 [31] J. Song, M. L. Gordin, T. Xu, S. Chen, Z. Yu, H. Sohn, J. Lu, Y. Ren, Y. Duan, D. Wang, *Angew.*
24 *Chem. Int. Ed.* **2015**, *54*, 4325.
25 [32] H. Xu, Y. Deng, Z. Zhao, H. Xu, X. Qin, G. Chen, *Chem. Commun.* **2014**, *50*, 10468.
26 [33] C. Tang, Q. Zhang, M.-Q. Zhao, J.-Q. Huang, X.-B. Cheng, G.-L. Tian, H.-J. Peng, F. Wei, *Adv.*
27 *Mater.* **2014**, *26*, 6100.
28 [34] F. Wu, J. Li, Y. Tian, Y. Su, J. Wang, W. Yang, N. Li, S. Chen, L. Bao, *Sci. Rep.* **2015**, *5*, 13340.
29 [35] S. Yuan, J. L. Bao, L. Wang, Y. Xia, D. G. Truhlar, Y. Wang, *Adv. Energy Mater.* **2016**, *6*,
30 1501733.
31 [36] G. Zhou, E. Paek, G. S. Hwang, A. Manthiram, *Nat. Commun.* **2015**, *6*, 7760.
32 [37] Y. J. Choi, B. S. Jung, D. J. Lee, J. H. Jeong, K. W. Kim, H. J. Ahn, K. K. Cho, H. B. Gu, *Phys.*
33 *Scripta* **2007**, *62*, T129.
34 [38] X. Ji, S. Evers, R. Black, L. F. Nazar, *Nat. Commun.* **2011**, *2*, 325.
35
36
37
38
39
40
41
42
43
44
45
46
47
48
49
50
51
52
53
54
55
56
57
58
59
60
61
62
63
64
65

- 1
2
3
4
5
6
7
8
9
10
11
12
13
14
15
16
17
18
19
20
21
22
23
24
25
26
27
28
29
30
31
32
33
34
35
36
37
38
39
40
41
42
43
44
45
46
47
48
49
50
51
52
53
54
55
56
57
58
59
60
61
62
63
64
65
- [39] X. Liang, C. Y. Kwok, F. Lodi-Marzano, Q. Pang, M. Cuisinier, H. Huang, C. J. Hart, D. Houtarde, K. Kaup, H. Sommer, T. Brezesinski, J. Janek, L. F. Nazar, *Adv. Energy Mater.* **2015**, *6*, 1501636.
- [40] X. Liang, C. Hart, Q. Pang, A. Garsuch, T. Weiss, L. F. Nazar, *Nat. Commun.* **2015**, *6*, 5682.
- [41] X. Wang, G. Li, J. Li, Y. Zhang, A. Wook, A. Yu, Z. Chen, *Energy Environ. Sci.* **2016**, *9*, 2533
- [42] X. Liang, L. F. Nazar, *ACS Nano* **2016**, *10*, 4192.
- [43] L. E. Greene, M. Law, D. H. Tan, M. Montano, J. Goldberger, G. Somorjai, P. Yang, *Nano Lett.* **2005**, *5*, 1231.
- [44] J. Liu, Y. Li, R. Ding, J. Jiang, Y. Hu, X. Ji, Q. Chi, Z. Zhu, X. Huang, *J. Phys. Chem. C* **2009**, *113*, 5336.
- [45] Y. Diao, K. Xie, S. Xiong, X. Hong, *Journal of Power Sources* **2013**, *235*, 181.
- [46] G. Xu, J. Yuan, X. Tao, B. Ding, H. Dou, X. Yan, Y. Xiao, X. Zhang, *Nano Res.* **2015**, *8*, 3066.
- [47] Q. Zhang, Y. Wang, Z. W. Seh, Z. Fu, R. Zhang, Y. Cui, *Nano Lett.* **2015**, *15*, 3780.

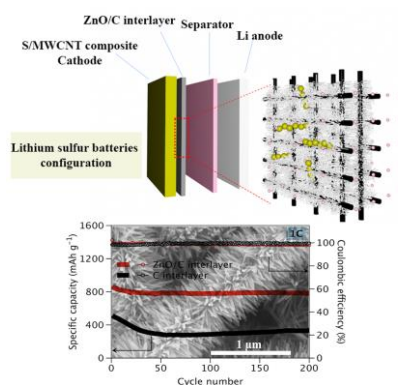
1 **A bio-inspired polysulfide adsorptive brush**, consisting of zinc oxide nanowires and
 2 conductive frameworks, has been designed and used as a chemi-functional interlayer to
 3 advance lithium sulfur batteries by effectively trapping and reutilizing migrating polysulfides.
 4 With the incorporation of this hierarchically nano-structured interlayer, good cycle stability
 5 and rate capability have been achieved for a readily-available sulfur/carbon nanotube
 6 composite cathode.

7
 8 **Keywords:** lithium sulfur batteries, brush-like interlayer, zinc oxide nanowires, conductive
 9 frameworks, polysulfides

10
 11
 12
 13 Teng Zhao[‡], Yusheng Ye[‡], Xiaoyu Peng[‡], Giorgio Divitini, Hyun-Kyung Kim, Cheng-Yen
 14 Lao, Paul R Coxon, Kai Xi, Yingjun Liu, Caterina Ducati, Renjie Chen*, R. Vasant Kumar*

15
 16
 17
 18 **Advanced lithium-sulfur batteries enabled by a bio-inspired polysulfide adsorptive**
 19 **brush**

20
 21
 22
 23 ToC figure



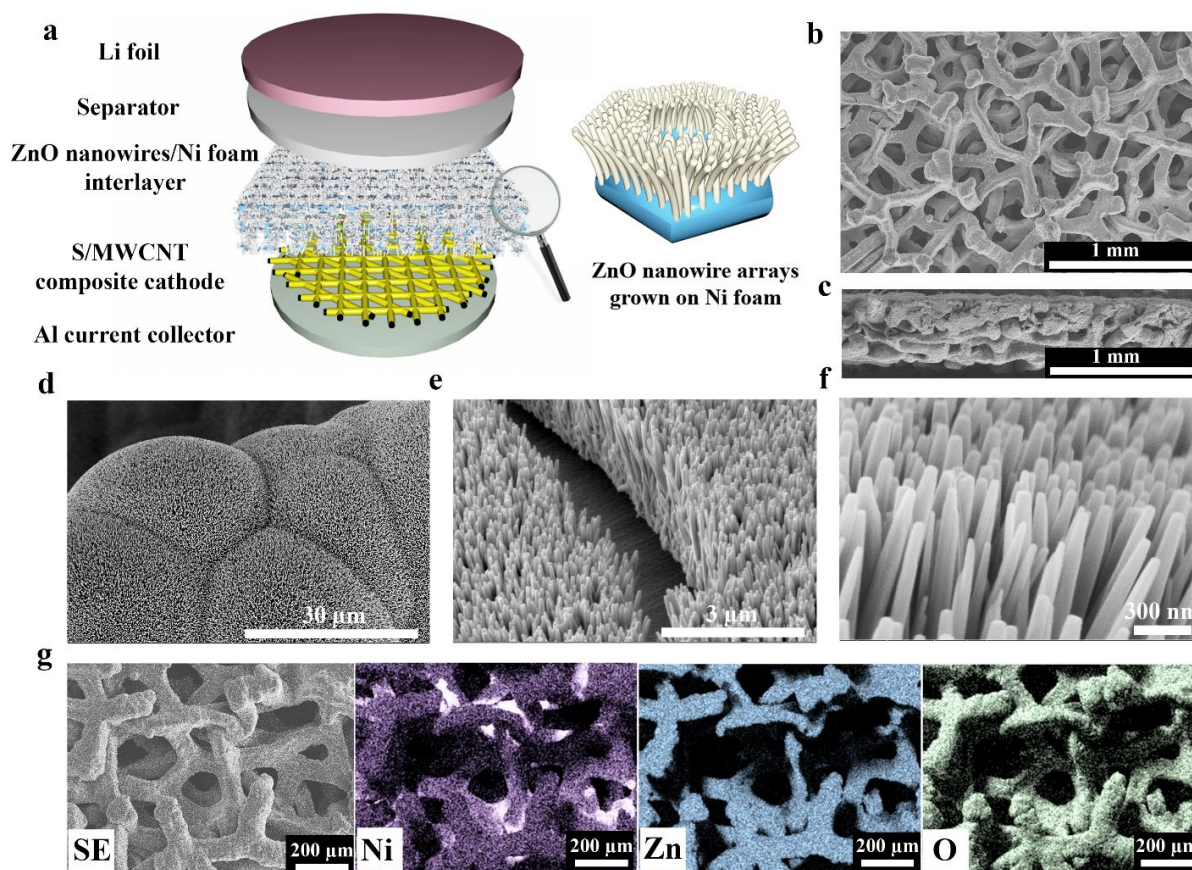


Figure 1. (a) Illustration of the assembled cell model, including a conceptual drawing of the ZnO nanowire arrays on the surface of Ni foam. (b) top-view and (c) Cross-section low magnification SEM images of the hybrid ZnO nanowires/Ni foam interlayer. (d-f) High-magnification SEM images of the hybrid ZnO nanowires /Ni foam interlayer. (g) Secondary electrons (SE) SEM image of the hybrid ZnO/Ni interlayer and the corresponding elemental maps.

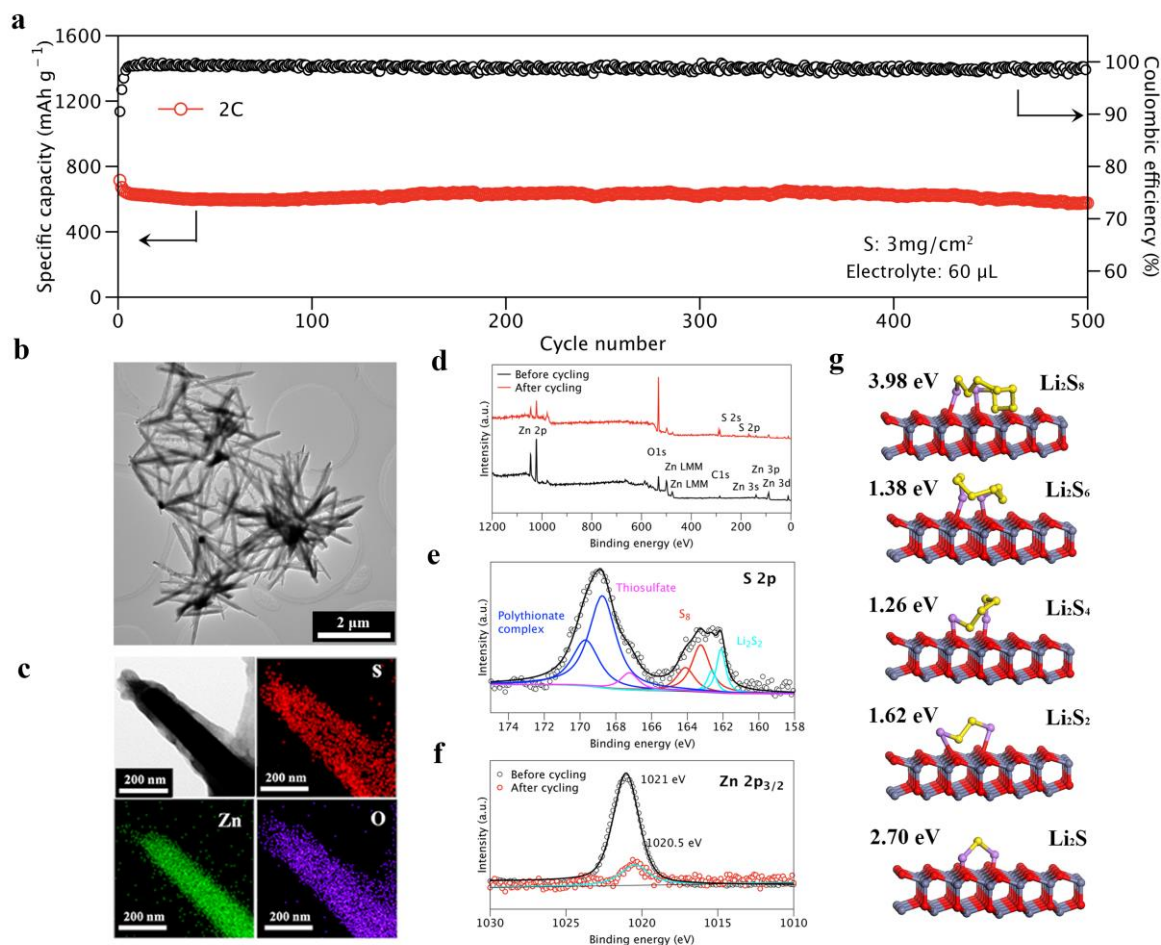


Figure 2. (a) Cycle performance of the Li-S cell with ZnO/Ni interlayer at 2C. (b) TEM image of cycled ZnO nanowires which were detached from the Ni foam by sonication. (c) TEM image of a single ZnO nanowire with a rough S-containing shell and corresponding elemental maps. (d) XPS survey spectra of hybrid ZnO/Ni interlayer before and after cycling (e) S2p XPS spectrum of the cycled hybrid interlayer. (f) Comparison of Zn 2p_{3/2} XPS spectrum of the hybrid interlayer before and after cycling. (g) Optimized configurations for the binding of five S species to the O-terminated polar surface of wurtzite ZnO crystal.

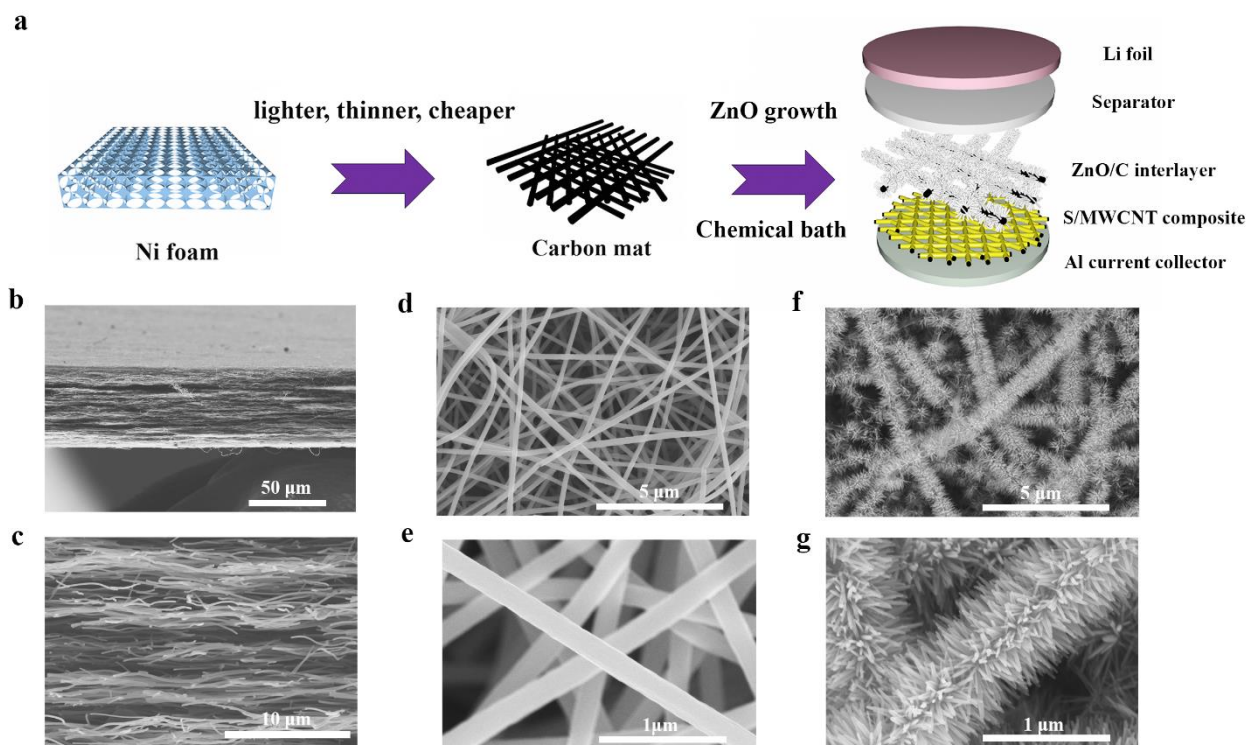


Figure 3. (a) Schematic of turning the Ni based conceptual interlayer to practical carbon based interlayer. (b-c) Cross-section low and high magnification SEM images of the carbon nanofiber interlayer. (d-e) Top-view low and high magnification SEM images of the carbon nanofiber interlayer. (f-g) Top-view low and high magnification SEM images of the hybrid ZnO nanowires/C nanofiber interlayer

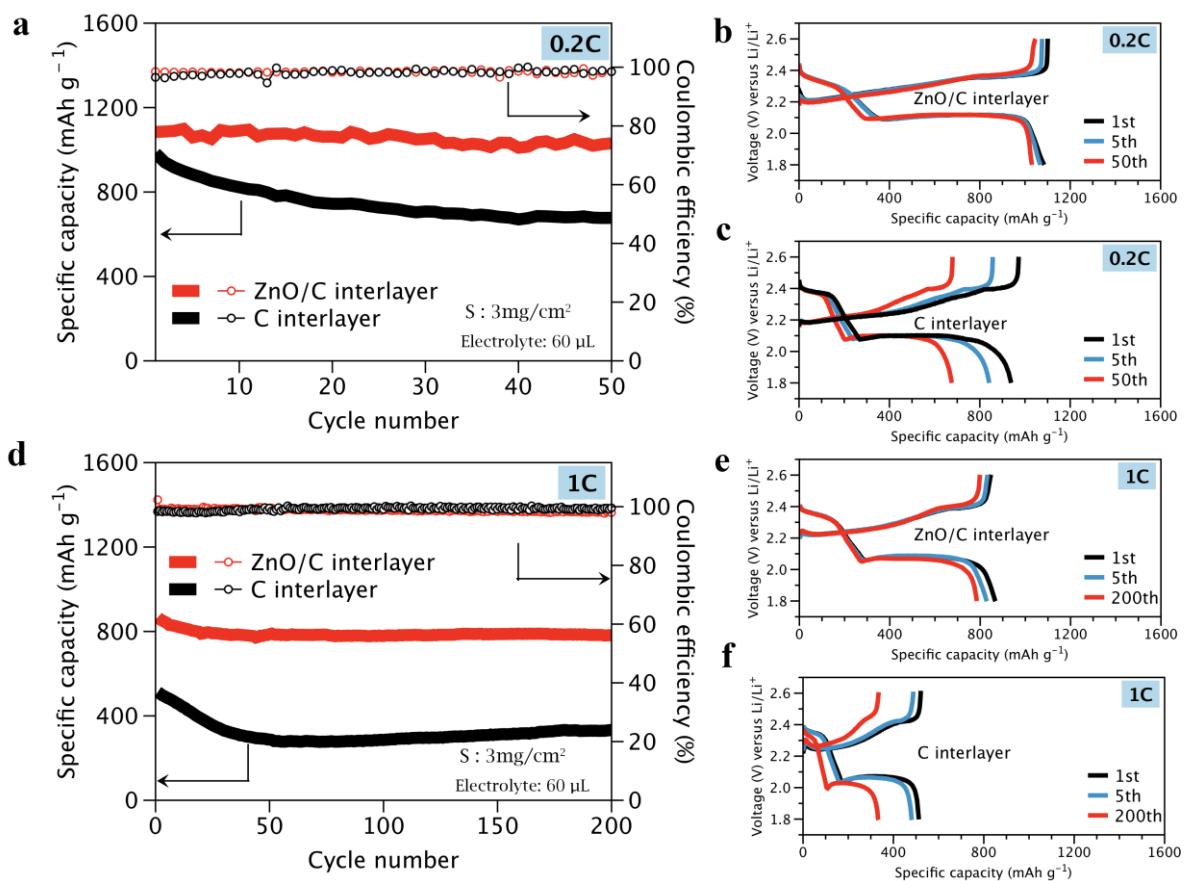


Figure 4. Cycle performance of the Li-S cell with different interlayers at current rate of (a) 0.2C and (d) 1C. Discharge-charge profiles of the Li-S cell with ZnO nanowires/carbon nanofiber interlayer after different cycles at (b) 0.2C and (e) 1C. Discharge-charge profiles of the Li-S cell with carbon nanofiber interlayer after different cycles at (c) 0.2C and (f) 1C.

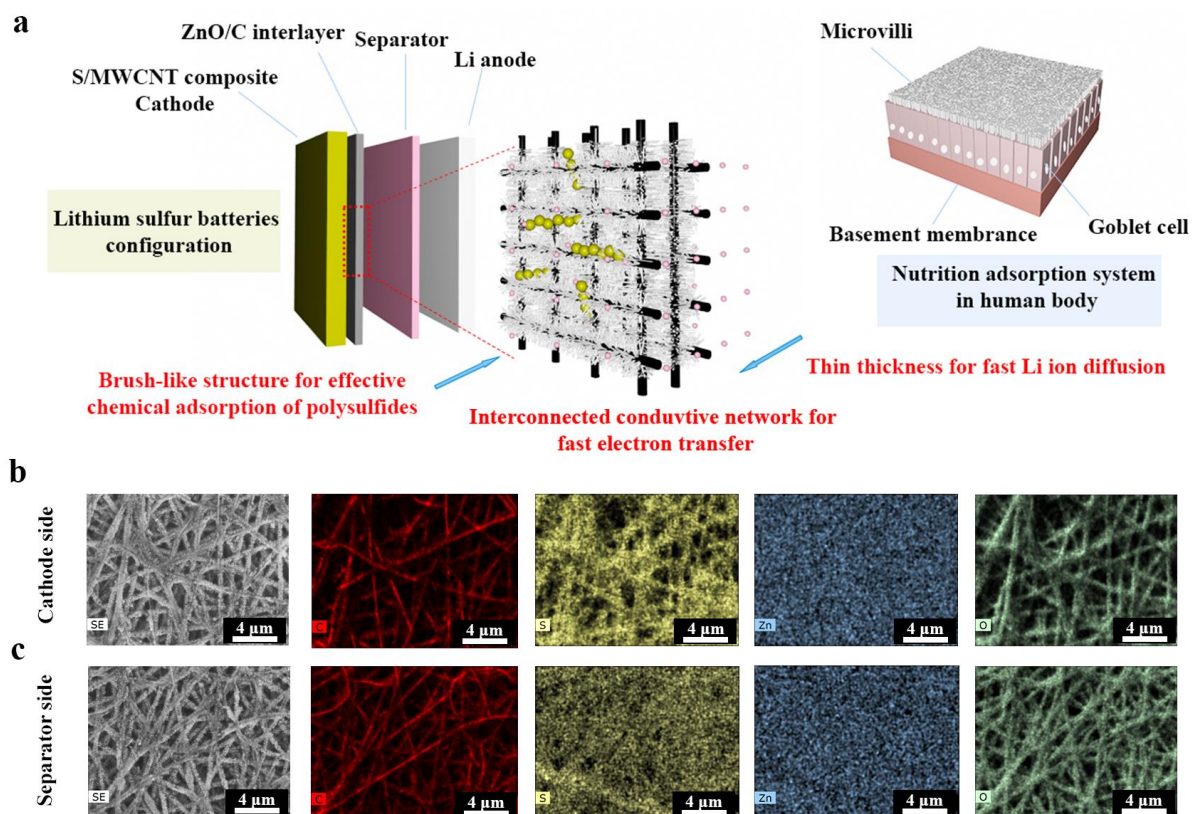
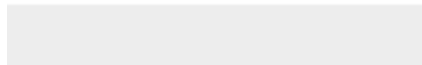
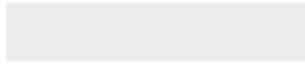


Figure 5. (a) Schematic of the structural and chemical function of the hybrid ZnO nanowires/carbon nanofibers interlayer in Li-S batteries, which mimic that of intestinal cell in human body. SEM image of the cycled hybrid ZnO nanowires/carbon nanofibers interlayer and corresponding elemental maps: (b) Cathode side (c) Separator side.



Click here to access/download
Production Data
Supporting information.docx





Click here to access/download

Production Data

Comments and Response.docx





Click here to access/download
Production Data
Figure 1.tif





Click here to access/download
Production Data
Figure 2.tif





[Click here to access/download](#)

Production Data
Figure 3.tif






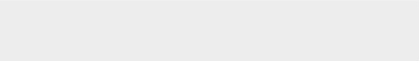

[Click here to access/download](#)

Production Data
Figure 4.tif





Click here to access/download
Production Data
Figure 5.tif





Click here to access/download
Production Data
TOC Figure.tif